JACS
JOURNAL OF THE AMERICAN CHEMICAL SOCIETY
Article
pubs.acs.org/JACS

Single Hydrogen Bond Donation from Flavin N_5 to Proximal Asparagine Ensures FAD Reduction in DNA Photolyase

I M. Mahaputra Wijaya,[†,#] Tatiana Domratcheva,[*,§,#] Tatsuya Iwata,[†,‡] Elizabeth D. Getzoff,[∥] and Hideki Kandori[*,†,‡]

[†]Department of Frontier Materials, and [‡]OptoBioTechnology Research Center, Nagoya Institute of Technology, Nagoya 466-8555, Japan

[§]Department of Biomolecular Mechanisms, Max Planck Institute for Medical Research, Jahnstrasse 29, Heidelberg 69120, Germany

[∥]Department of Integrative Structural and Computational Biology and The Skaggs Institute for Chemical Biology, The Scripps Research Institute, La Jolla, California 92037, United States

Supporting Information

ABSTRACT: The spread of the absorbance of the stable $FADH^{\bullet}$ radical (300−700 nm) allows CPD photolyase to highly efficiently form $FADH^{-}$, making it functional for DNA repair. In this study, FTIR spectroscopy detected a strong hydrogen bond, from FAD N_5−H to the carbonyl group of the Asn378 side chain, that is modulated by the redox state of FAD. The observed characteristic frequency shifts were reproduced in quantum-mechanical models of the flavin binding site, which were then employed to elucidate redox tuning governed by Asn378. We demonstrate that enhanced hydrogen bonding of the Asn378 side chain with the $FADH^{\bullet}$ radical increases thermodynamic stabilization of the radical state, and further ensures kinetic stabilization and accumulation of the fully reduced $FADH^{-}$ state.

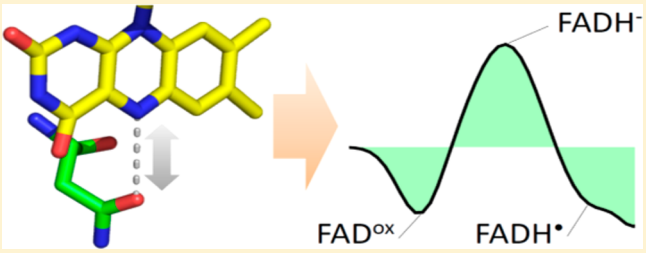

INTRODUCTION

Ultraviolet (UV) radiation from the sun can create lesions in DNA. UV-induced photoreactions of DNA produce two major forms of damage: cyclobutane pyrimidine dimer (CPD) and the (6−4) pyrimidine pyrimidone photoproduct ((6−4)PP).[1] These lesions block DNA replication and translation, resulting in mutagenesis or tumorigenesis.[2] Photolyase enzymes are powered by near UV or blue light (350−450 nm) to directly repair DNA.[3] Two distinct enzymes, CPD photolyase and (6−4) photolyase, specifically repair CPD and (6−4)PP, respectively.[4,5] Photolyases possess flavin adenine dinucleotide (FAD) as a common catalytic cofactor that is noncovalently bound inside the protein,[6,7] and a second cofactor that is usually a derivative of folate or deazaflavin, assisting the FAD chromophore as a photoantenna through energy transfer.[8,9] During repair, photolyase flips the lesion from the DNA double helix and positions it next to FAD, which is situated at the bottom of the DNA binding cavity.[10]

To form the catalytically competent state of photolyase, light-excited oxidized FAD^{ox} can receive electrons through a triple tryptophan cascade that wires FAD to its surrounding environment.[11] In vivo, CPD photolyase from *Escherichia coli* (*E. coli*) possesses catalytically active, fully reduced $FADH^{-}$, but the protein is usually purified in the semiquinoid state $FADH^{\bullet}$ in vitro.[12] CPD photolyases from *E. coli* and *Thermus thermophilus* are stable in the $FADH^{\bullet}$ state for several days in solution without an external electron donor.[8,13] Accumulation of the $FADH^{\bullet}$ state was also observed in the photolyase homologues cryptochrome CPH1 and aCRY from *Chlamydomonas reinhardtii*.[14,15] The $FADH^{\bullet}$ state is characterized by broad absorbance in the range 300−700 nm,[16] which enables these proteins to efficiently capture light of any wavelength in this wide spectral region. Illumination results in the highly efficient reduction (i.e., photoactivation) of $FADH^{\bullet}$ to $FADH^{-}$, which is functional for DNA repair in *E. coli* photolyase.[3,12] However, the mechanism by which the neutral radical $FADH^{\bullet}$ is stabilized by its surrounding residues is not clearly understood.

It has been proposed that the N_5−H group present in both $FADH^{-}$ and $FADH^{\bullet}$ states becomes stabilized by a strong hydrogen bond in the $FADH^{\bullet}$ state.[17] The asparagine (Asn) residue in the position proximal to N_5 of FAD is commonly conserved in all members of class I CPD and (6−4) photolyase,[18,19] cryptochrome DASH,[20] and some of class II photolyases.[21−23] Previously, a kinetic barrier for rate-limiting deprotonation of N_5 by a proximal residue and an Asn switching movement upon the FAD reduction-protonation step were proposed.[24] The importance of Asn in proximity of N_5 was demonstrated by mutation of this Asn into serine in *E. coli* CPD photolyase which causes the loss of the $FADH^{\bullet}$ state together with DNA repair ability.[25] Furthermore, mutation of

Received: October 8, 2015
Published: March 22, 2016

DOI: 10.1021/jacs.5b10533
J. Am. Chem. Soc. 2016, 138, 4368−4376

Asp to Asn in the equivalent position in *Arabidopsis* cryptochrome AtCry1 reverts light-induced $FADH^{\bullet}$ accumulation and CPD repair ability.[26] These data indicate that Asn, positioned with its amide side-chain carbonyl and amine groups near FAD N_5, may play a functional role in the stabilization of $FADH^{\bullet}$ required for further functional reduction to $FADH^{-}$.

In this study, we examined the conformations of the FAD N_5-proximal Asn378 in *E. coli* CPD photolyase through changes of its side chain hydrogen bonding network. Light-induced FAD reduction was analyzed by Fourier transform infrared (FTIR) difference spectroscopy as it is a sensitive method to study conformational changes in the hydrogen-bonding environment of photoreceptive proteins.[27−29] Changes of the Asn378 bond stretches of both carbonyl and amine groups, resulting from the changes in the hydrogen bonding networks upon light-induced FAD reduction and N_5 protonation, can be revealed by isotope labeling. To identify the changes, we prepared the CPD photolyase enzyme, which was unlabeled, uniformly ^{13}C-labeled and ^{13}C-labeled with all Asn residues unlabeled (denoted as "Asn reverse-labeled"). The C═O stretch of the Asn side chain shows infrared (IR) absorbance at 1677−1678 cm^{-1}.[30] In the Asn reverse-labeled enzyme, C═O stretches from all amino acid residues other than Asn become downshifted by 35−40 cm^{-1}. This would enable to identify the C═O stretches from Asn residues in the "cleared" frequency region >1670 cm^{-1}.[31] Because of the strong IR absorbance of the C═O stretch of the Asn side chain, changes to the hydrogen bonding network of this residue should be observed in the FTIR spectrum. The double difference spectrum of isotope-labeled samples upon photoactivation would further confirm the existence of less intense signals from the amino group of the side chain if changes to its hydrogen bonding network occur. In the <1670 cm^{-1} region, changes of the N−H bending and C−N stretch of the Asn side chain can also be observed. Out of 20 Asn residues in *E. coli* CPD photolyase, only Asn378 exists near N_5 of FAD,[32] excluding the possibility that the remaining Asn residues are involved in FAD photoactivation. Upon light-induced FAD reduction, the Asn378 side chain interacting with N_5 of FAD is expected to show a similar frequency in both Asn reverse-labeled and unlabeled enzymes. This Asn signal, however, should be absent in the spectrum of the uniformly ^{13}C-labeled enzyme. It should be noted that an unlabeled Asn residue possesses the unlabeled backbone C═O group whose signal should appear in the amide I region.

The sensitivity of FTIR spectroscopy used to observe changes in the Asn378 hydrogen bonding network might reflect minute differences in conformations which cannot be observed in crystal structures. Thus, to deepen our understanding of the details of Asn378 conformations upon FAD reduction we performed quantum chemical normal-mode analysis and energy calculations using the *E. coli* photolyase crystal structure (PDB ID: 1DNP).[32] We first used calculations to confirm our experimental assignments of the Asn378 vibrations. Further we performed a comparison of redox energies to link the changes identified in the FTIR spectra to the stabilization of the $FADH^{\bullet}$ and $FADH^{-}$ states crucial for the photolyase DNA repair function.

EXPERIMENTAL AND COMPUTATIONAL METHODS

UV−Visible and FTIR Spectroscopy. *Sample Preparation.* For UV−visible and FTIR measurements, the CPD photolyase E109A mutant, which cannot bind the 5,10-methenyltetrahydrofolate (MTHF) photoantenna chromophore, prepared at natural isotope abundance and in the ^{13}C rich media as previously described with a slight modification (see Supporting Information for details).[16] The enzyme in the semiquinoid $FADH^{\bullet}$ and fully oxidized FAD^{ox} in storage buffer was exchanged into measurement buffer [50 mM HEPES, 100 mM NaCl, 5% glycerol, pH 7.0] containing 25 mM ($FADH^{\bullet}$) and 50 mM (FAD^{ox}) of β-mercaptoethanol, concentrated through Amicon centrifugation devices (Millipore) at 4 °C, and set at a final concentration of approximately 2 mM. This concentration facilitates detection of photolyase photoactivation since CPD photolyase cannot be dried to minimize strong IR water absorption. Sample concentration was determined from the absorbance of free FAD at 450 nm by UV−visible spectroscopy (data not shown). Samples were placed in a BaF_2 window by pipetting, sandwiched by another BaF_2 window, then sealed with Parafilm (Pechiney Plastic Packaging).

UV−Visible and FTIR Measurements. FTIR measurements were conducted by an FTS-7000 instrument (DIGILAB) which was equipped with an Optistat-DN cryostat (Oxford Instruments) and an ITC-4 temperature controller (Oxford Instruments). The UV−visible spectra were recorded with a V-550DS spectrometer (JASCO) that was also equipped with an Optistat-DN cryostat and a ITC-4 temperature controller as previously described.[16]

For the samples resting in the semiquinoid state, spectra of the unphotolyzed sample were recorded. Samples were illuminated with a 300 W xenon lamp (Max-302, ASAHI SPECTRA) with a >550 nm filter for 2 min, then light-induced FAD reduction spectra were recorded. The corresponding recorded UV−visible difference spectra of the $FADH^{\bullet}$ conversion into $FADH^{-}$ (after illumination minus before illumination), exemplified by the unlabeled sample, is shown in Supporting Figure S1.

Separately, the samples resting in the oxidized form were first illuminated using a >550 nm filter to remove the portion of the enzyme resting in the semiquinoid state. This yielded sample composed of the fully reduced enzyme and oxidized enzyme without the presence of the semiquinoid form (spectra not shown). The UV−visible and FTIR spectra were then recorded (α) and the samples were subsequently illuminated with a >390 nm filter for 2 min to induce the reduction of FAD^{ox} to $FADH^{-}$. Inevitably a small amount of transiently formed $FADH^{\bullet}$ was generated, which was further converted to $FADH^{-}$ by illumination with a >550 nm filter for 30 s. The photolyzed spectra were recorded (β), and the difference spectra (β minus α) were produced. These difference spectra represent the complete photoconversion of FAD^{ox} into $FADH^{-}$ with only a negligible amount of $FADH^{\bullet}$ being formed. The corresponding recorded UV−visible difference spectra of the conversion of FAD^{ox} into $FADH^{-}$ (β minus α), as exemplified by an unlabeled sample, is shown in Supporting Figure S2.

Computational Details. *Geometry Optimization and Vibrational Analysis.* Initial atomic coordinates of the heavy atoms in the photolyase active site models were assigned based on the *E. coli* photolyase crystal structure (PDB ID: 1DNP, molecule A).[32] In the models, we included the entire FAD cofactor and Asn378 residue together with a large number of residues forming the FAD binding site. Hydrogen atoms were added with ViewerPro 4.2 software (Accelrys Inc.). The following protonation states of the acidic/basic groups were modeled: Asp372, Asp374 and Glu363 were deprotonated, Arg344 was protonated, in the FAD molecule, one phosphate was protonated and the other phosphate was deprotonated. The chosen protonation states resulted in a total charge of −3 in the FAD^{ox} and $FADH^{\bullet}$ models and −4 in the $FADH^{-}$ model. Altogether, the models consist of 299 atoms (FAD^{ox} state) and 300 atoms ($FADH^{\bullet}$ and $FADH^{-}$ states). The geometry was optimized with the (U)B3LYP/6-31G* density functional theory method with coordinates of 10 atoms frozen (Supporting Figure S3) in order to mimic the constraints in the protein. The harmonic vibrational frequencies and IR intensities were computed at the optimized geometries. To estimate the vibrational frequencies of the Asn378 side chain interacting with flavin in our rather large models, only displacements of atoms comprising the Asn378 side chain and the lumiflavin portion of FAD

DOI: 10.1021/jacs.5b10533
J. Am. Chem. Soc. 2016, 138, 4368−4376

(40/41 atoms depending on flavin protonation) were computed to obtain the Hessian matrix. To minimize contributions from the two terminal atoms (C1′ of lumiflavin and Cα of Asn378) to the computed normal modes, large 500 au masses were assigned to these atoms. To model isotope-labeling, the frequencies and IR intensities were recomputed with ^{13}C substitutions. The IR spectra were simulated by convoluting the harmonic frequencies (scaled by 0.965) and IR intensities with Lorenzian functions of a 8 cm^{-1} width. All quantum-chemical calculations were performed with the Firefly program,[33] which is partially based on the US GAMESS program.[34]

Calculations of Redox Energies. We compared redox energies of the above-described photolyase models containing Asp378, the models containing Ala378 instead of Asp378 and a complex of lumiflavin combined with 6 water molecules (LfH−6H_2O). The Ala378 models were derived from the Asn378 models by substituting the amide group $CONH_2$ with a hydrogen atom (placed along the C−C bond with the C−H distance of 1.08 Å) without further geometry optimization. The optimized geometries of the LfH−6H_2O model are shown in Supporting Figure S4.

To derive the redox energies characterizing the FADH$^\bullet$ to FADH$^-$ reduction (or LfH$^\bullet$ to LfH$^-$ reduction), the vertical energies were computed in the FADH$^-$ (LfH$^-$) and FADH$^\bullet$ (LfH$^\bullet$) states at the geometries optimized in the FADH$^\bullet$ (LfH$^\bullet$) and FADH$^-$ (LfH$^-$) states, respectively. The vertical energies together with the energies of the minima (four energies for each model indicated as E(state of energy calculation//state of geometry optimization)) were used to compute the three redox energies considered in our analysis: adiabatic electron affinity (AEA), reorganization energy in the fully reduced state (λ_1) and reorganization energy in the semiquinone radical state (λ_2).

$$\mathrm{AEA} = E(\mathrm{FADH^{\cdot}//FADH^{\cdot}}) - E(\mathrm{FADH^{-}//FADH^{-}})$$

$$\lambda_1 = E(\mathrm{FADH^{-}//FADH^{\cdot}}) - E(\mathrm{FADH^{-}//FADH^{-}})$$

$$\lambda_2 = E(\mathrm{FADH^{\cdot}//FADH^{-}}) - E(\mathrm{FADH^{\cdot}//FADH^{\cdot}})$$

To compare the redox energies, the energies of the fully reduced and radical states E(FADH$^-$) and E(FADH$^\bullet$), respectively, were approximated with parabolas intersecting along the flavin reduction/oxidation coordinate Q.

$$E(\mathrm{FADH^{-}}) = Q^2$$

$$E(\mathrm{FADH^{\cdot}}) = (\lambda_2/\lambda_1)(Q - \lambda_1^{1/2})^2 + \mathrm{AEA}$$

To include flavin photoexcitation in the analysis, the excited radical state E(FADH$^\bullet$*) was considered to be 44 kcal/mol upshifted with respect to the radical state E(FADH$^\bullet$), which corresponds to an excitation maximum at 650 nm.

$$E(\mathrm{FADH^{\cdot}*}) = (\lambda_2/\lambda_1)(Q - \lambda_1^{1/2})^2 + \mathrm{AEA} + 44$$

RESULTS AND DISCUSSION

FTIR Study of Asn378-FAD Interactions upon Photoactivation. The unphotolyzed radical FADH$^\bullet$ enzyme undergoes a one-electron reduction to FADH$^-$ upon photoactivation. This may trigger the FADH$^-$ butterfly bending together with conformational changes of the residues surrounding FAD. Here we focus on observing the changes of the N_5-proximal Asn378 by noting signals of its side chain stretches. The difference FTIR spectra of Asn reverse-labeled (blue) and unlabeled (black) enzyme in the 1740−1420 cm^{-1} region are shown in Figure 1a. The UV−visible difference spectrum of the photoconversion from FADH$^\bullet$ to FADH$^-$ of the unlabeled enzyme is shown in Supporting Figure S1.

When comparing the FTIR spectra in Figure 1a, the unshifted peak at 1677 (+) cm^{-1} can be seen in the clear region resulting from downshifting of the other peaks by

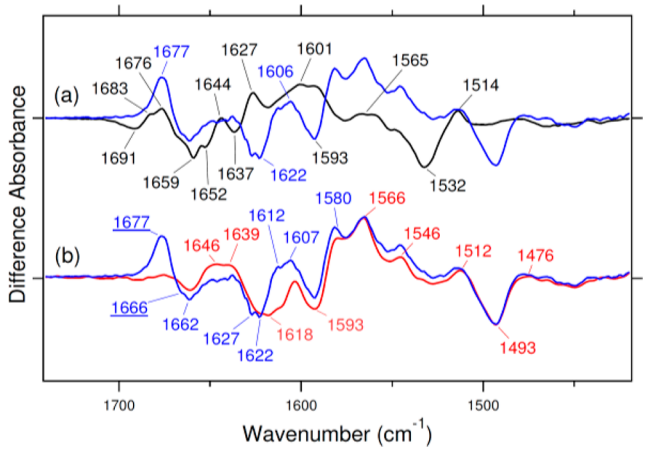

Figure 1. FTIR spectra of photoactivation from FADH$^\bullet$ to FADH$^-$ of unlabeled (black), Asn reverse-labeled (blue), and uniformly ^{13}C-labeled (red) samples. One division equals 0.01 absorbance units (au).

isotopic ^{13}C labeling in the Asn reverse-labeled (blue) spectrum. The positive peak at 1677 cm^{-1} is a good candidate for the C=O stretch of the Asn378 side chain.[29] The increased intensity at 1677 cm^{-1} in the Asn reverse-labeled spectrum (blue) indicates that another negative signal originating from the enzyme is overlapping with the Asn signal in the unlabeled sample spectrum (black). The absence of another signal at a frequency higher than 1677 cm^{-1} clearly indicates that the peak at 1677 (+) cm^{-1} (blue) was upshifted upon photoactivation, suggesting that either a shoulder at 1666 (−) or a peak at 1662 (−) cm^{-1} corresponds to the Asn C=O stretch in the unphotolyzed FADH$^\bullet$ enzyme. To reveal whether the 1677 (+) peak pairs with the signals at 1666 (−) or 1662 (−) cm^{-1}, Asn reverse-labeled enzyme (blue) was compared with uniformly ^{13}C-labeled enzyme (red), as shown in Figure 1b. The peak at 1677 (+) cm^{-1} (underlined) is indeed absent from the uniformly ^{13}C-labeled spectrum (red). The peak at 1666 (−) is also absent in the uniformly ^{13}C-labeled enzyme (red), but it is likely that the peak at 1662 (−) cm^{-1} (red) still exists. Thus, the 1677 (+) cm^{-1} peak and the shoulder at 1666 (−) cm^{-1} of the blue spectrum (underlined) originate from the unlabeled Asn C=O stretch revealing an upshift of the frequency upon photoactivation. In Figure 1b, the peak at 1646 (+) cm^{-1} in the uniformly ^{13}C-labeled spectrum (red) probably corresponds to the shoulder at 1683 (+) cm^{-1} of the unlabeled spectrum (black) in Figure 1a, which undergoes a downshift upon ^{13}C-labeling. The double difference spectrum corresponding to Figure 1b is shown in Supporting Figure S3.

The identified positive 1677 cm^{-1} peak represents the C=O stretch of Asn378 in the FADH$^-$ form. This frequency is in agreement with a previously reported C=O stretch of Asn.[29] The negative peak at 1666 cm^{-1} represents the C=O stretching of Asn378 in the neutral FADH$^\bullet$ radical form. As previously proposed by Damiani et al., the C=O group of Asn378 points toward N_5−H of the FADH$^\bullet$ radical and forms a hydrogen bond.[25] The low frequency of the 1666 cm^{-1} peak implies that the C=O group of Asn378 is strongly hydrogen bonded with the N_5−H group stabilizing the radical state, as previously proposed.[17] The upshift of the signal upon photoactivation indicates that the hydrogen bond between the Ans378 carbonyl oxygen and the N_5−H proton might become slightly weaker with a longer distance after formation of the FADH$^-$ state. Asn378 may rotate its side chain in a

DOI: 10.1021/jacs.5b10533
J. Am. Chem. Soc. 2016, 138, 4368−4376

movement that is opposite to that previously proposed for FAD^{ox} to $FADH^{\bullet}$ reduction[25] or it may simply be slightly tilted. The peak at 1666 cm^{-1} is significantly lower than 1680 cm^{-1} previously observed in water.[35] The lower frequency could be explained by a specific conformation of Asn378 enabling strong interactions in the photolyase $FADH^{\bullet}$ state, whereas weaker interactions, and possibly multiple hydrogen bonding arrangements could exist in water. To our knowledge, the 1666 cm^{-1} frequency is the lowest frequency C=O stretch of an Asn side chain to be observed thus far by FTIR spectroscopy.

To characterize the conformation of Asn378 in each redox state of the photolyase enzyme, not only photoactivation from $FADH^{\bullet}$ to $FADH^{-}$, but also light-induced reduction from the fully oxidized state FAD^{ox} to $FADH^{-}$ was measured. The aim was to observe changes in the conformation of the Asn378 side chain when unprotonated N_5 of FAD^{ox} becomes protonated N_5–H of $FADH^{-}$. The FTIR spectral measurements of the oxidized Asn reverse-labeled enzyme (blue) and unlabeled enzyme (black) in the 1740–1420 cm^{-1} region are shown in Figure 2a. The corresponding difference UV–visible spectrum

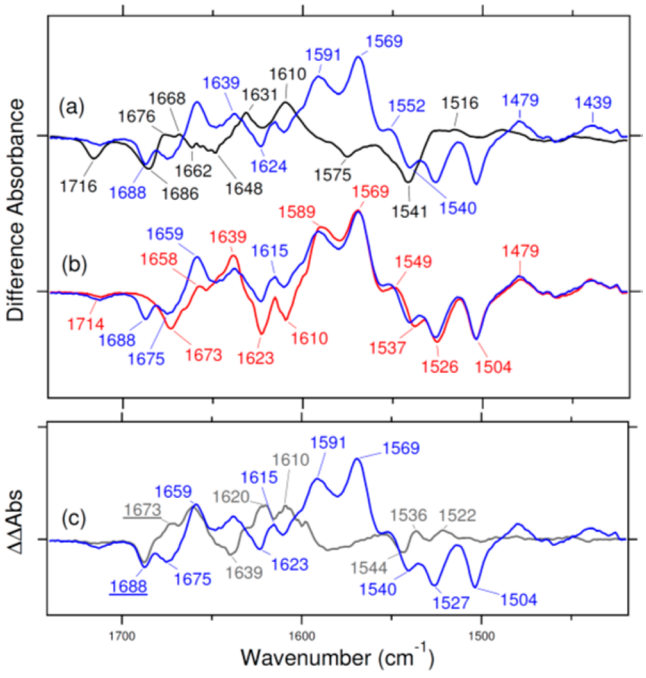

Figure 2. FTIR spectra of photoactivation from FAD^{ox} to $FADH^{-}$ of unlabeled (black), Asn reverse-labeled (blue), uniformly ^{13}C-labeled (red) samples (a,b,c), and double difference (gray) spectrum (blue minus red) (c). One division equals 0.01 au.

of the unlabeled enzyme confirming photoactivation of FAD^{ox} to the fully reduced $FADH^{-}$ state that is similar to the one obtained upon $FADH^{\bullet}$ photoreduction, with only a negligible accumulation of $FADH^{\bullet}$ is shown in Supporting Figure S2. In Figure 2a, the C=O stretches of all Asn residues should appear at similar frequencies in both spectra. Thus, the most plausible candidate for the Asn378 C=O stretch is the signal at 1688 (−) cm^{-1} in the Asn reverse-labeled spectrum (blue). However, the unlabeled spectrum (black) showed a similar negative peak at a slightly lower frequency 1686 (−) cm^{-1}, indicating that another signal originating from a different moiety also appears at this frequency. The negative peak at 1688 cm^{-1} (blue/underlined) was confirmed to originate from the Asn C=O stretch by comparing the Asn reverse-labeled enzyme (blue) with the uniformly ^{13}C-labeled enzyme (red), as shown in Figure 2b. In the uniformly ^{13}C-labeled spectrum (red), no signal exists around 1688 (−) cm^{-1}. This confirms that the 1688 cm^{-1} peak of the Asn reverse-labeled spectrum does not originate from a higher frequency signal that is shifted due to ^{13}C labeling. Rather, the 1688 cm^{-1} peak corresponds to the C=O stretch of Asn378 in the FAD^{ox} state.

Since photoreduction of FAD^{ox} leads to the $FADH^{-}$ state similar to that in the measurements of photoactivation starting from the $FADH^{\bullet}$ state, the Asn378 positive peak should be detected at a similar frequency in our two photoreduction experiments. Therefore, we expect a downshifted Asn378 C=O stretch in the $FADH^{-}$ state as compared to that in the FAD^{ox} state. From the spectra presented in Figure 2b, clues for the pairing positive peak can be obtained from the difference in the intensity of two negative peaks at 1675 (−) (blue) and 1673 (−) cm^{-1} (red). Since the negative peak at 1675 cm^{-1} of the Asn reverse-labeled spectrum (blue) includes the contribution of the uniformly ^{13}C-labeled spectrum plus a positive peak of the shifted Asn378 C=O stretch in the $FADH^{-}$ state, the existence of the latter can be revealed by subtraction of the uniformly ^{13}C-labeled spectrum from the Asn reverse-labeled spectrum (blue minus red) which results in the double difference spectrum (gray) shown in Figure 2c. The double difference spectrum shows a positive peak at 1673 cm^{-1} (underlined) corresponding to the Asn378 C=O stretch downshifted by interactions with N_5–H in the $FADH^{-}$ state. The 1673 (+) cm^{-1} peak is in good agreement with the 1677 (+) cm^{-1} peak (blue) in Figure 1 despite the 4 cm^{-1} difference.

The revealed change in the Asn378 C=O stretch in the three redox states of the photolyase enzyme summarized in Table 1 indicates formation of stronger and weaker hydrogen

Table 1. Asn378 C=O Frequencies in the Three Redox States of *E. coli* Photolyase

state	frequency (cm^{-1})
FAD^{ox}	1688
$FADH^{\bullet}$	1666
$FADH^{-}$	1677/1673

bonds of the Asn378 C=O group with N_5–H in the $FADH^{\bullet}$ and $FADH^{-}$ states, respectively. In the FAD^{ox} state, the Asn378 C=O side chain cannot form a hydrogen bond with N_5; therefore, it may interact with another group from the enzyme active site; however, the interactions are weaker than those with N_5–H upon photoreduction. Despite our data documenting the changes of the Asn378 C=O stretch caused by the differences in hydrogen bonding, it does not yet enable us to fully determine whether the Asn378 side chain rotates upon FAD reduction.

In the FTIR spectra presented in Figures 1 and 2, the differences in the amide I region of the Asn reverse-labeled and uniformly ^{13}C-labeled enzyme resulted from the protein backbone containing ^{12}C and ^{13}C atoms (Asn reverse-labeled) or only ^{13}C atoms (uniformly ^{13}C-labeled). Moreover, the spectral shifts indicate incomplete labeling of the FAD cofactor in our samples. In Figure 2a, the negative peak at 1716 cm^{-1} in the unlabeled spectrum (black) is likely to be shifted to 1673 cm^{-1} in the uniformly ^{13}C-labeled spectrum (red). These peaks correspond to the C_4=O stretch of FAD^{ox}. However, both Asn reverse-labeled (blue) and uniformly ^{13}C-labeled (red) spectra

DOI: 10.1021/jacs.5b10533
J. Am. Chem. Soc. 2016, 138, 4368–4376

in Figure 2a still show a negative peak at 1714 cm^{-1}, indicating that some fraction of the sample remained unlabeled. The enzyme was made with 99.0% pure ^{13}C glucose (Cambridge Isotope), but *E. coli* might efficiently utilize the 1% of the ^{12}C glucose content. On the basis of the small intensity of the remaining peaks at 1714 cm^{-1} relative to other major peaks, sample impurities due to incomplete labeling should not exceed 10%, and we firmly believe that more than 90% of the enzyme used in this experiment were successfully labeled with ^{13}C isotope.

To completely determine the conformation of Asn378 in each FAD state, observation of the C−N stretch and N−H bending of the Asn side chain is necessary. If the Asn378 side chain rotates, then not only a change to its carbonyl C═O stretch, but also changes to the -NH_2 vibrations should be observed. Otherwise, if the conformational change of Asn378 involves tilting instead of rotation, the change of the C−N stretch should not appear in the spectrum. The signal of the NH_2 plane bending at around 1612−1622 cm^{-1},[29] is difficult to determine in our labeling experiments due to appearing in this spectral region the differences in vibrations of the protein backbone containing both ^{13}C and ^{12}C isotopes in the Asn reversed labeled enzyme and only ^{13}C isotopes in the uniformly ^{13}C labeled enzyme. The FTIR frequency of the Asn C−N stretch is yet to be determined, but would likely appear at around 1250−1020 cm^{-1} similar to an aliphatic amine instead of at 1335−1250 cm^{-1} of an aromatic amine.[29] The small intensity expected for the C−N stretch signal should be still possible to detect in the double difference spectrum using ^{13}C-labeling. In contrast, if conducted by uniform and Asn reverse-^{15}N-labeling, detection of the signal could be complicated by an overlap of the C−N stretch signal with the other 3−4 cm^{-1} shifted signals induced by ^{15}N-labeling.

To identify the C−N stretch signal of Asn378, the lower-frequency region at 1420−1000 cm^{-1} of the Asn reverse-labeled (blue) and uniformly ^{13}C-labeled (red) from both photoreduction experiments starting from the $FADH^{\bullet}$ and FAD^{ox} states were compared in Figures 3a and 3b, respectively. The double difference spectra (blue minus red) shown in Figure 3c (gray for $FADH^{\bullet}$ to $FADH^{-}$ reduction and red for FAD^{ox} to $FADH^{-}$ reduction) should reveal the signal from the C−N stretch if Asn378 rotates. The rotation should yield a signal featuring positive and negative peaks in the double difference spectrum. However, the double difference spectrum (gray and red) in Figure 3c do not contain signals that could be attributed to the C−N stretch. Thus, no difference in the Asn378 NH_2 group hydrogen bonding environment could be proposed. We concluded that upon enzyme photoactivation, Asn378 does not undergo rotation, but may simply be tilting its side chain, adjusting the position of its C═O group with respect to the N_5−H group.

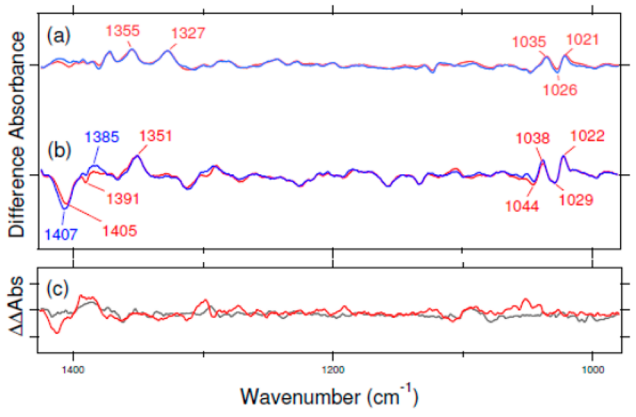

Figure 3. FTIR spectra of photoactivation of Asn reverse-labeled (blue) and uniformly ^{13}C-labeled (red) samples from $FADH^{\bullet}$ to $FADH^{-}$ (a), from FAD^{ox} to $FADH^{-}$ (b), and double difference spectra (red: blue minus red of FAD^{ox} to $FADH^{-}$, gray: blue minus red of $FADH^{\bullet}$ to $FADH^{-}$) (c). One division equals 0.01 au (upper panel) and 0.001 au (lower panel).

Computational Study of Asn378−FAD Interactions. Although the spectral shifts attributed to the C═O stretch of Asn378 are rather pronounced, the extent of the conformational change upon enzyme photoactivation might not be large. Because of the sensitivity of the FTIR spectroscopy, a sub-Å difference in hydrogen bonding distances of the Asn378 side chain upon its tilting inside the enzyme might be detected. Yet, this sub-Å difference might be critical to stabilize both the $FADH^{\bullet}$ and $FADH^{-}$ states of the enzyme. The Asn378 tilting motion coupled with the butterfly bending motion of the reduced flavin might result in minute structural differences which are indistinguishable in the crystal structures. To comprehend the details of the Asn378 conformation in each FAD state and to understand the functional relevance of the hydrogen bond changes, we characterized the Asn378 interactions in the photolyase enzyme employing quantum-chemical calculations. Using the crystal structure,[32] we developed computational models of *E. coli* photolyase in the three redox states characterized in our FTIR study. In the crystal structure, the Asn378 carbonyl group interacts with flavin N_5−H and also with tryptophan Trp382, as indicated in Figure 4. The distances characterizing these interactions in our computed models undergo changes depending on the flavin redox state as documented in Table 2. The flavin−Asn378 hydrogen bond is formed only with N_5−H of the $FADH^{\bullet}$ and $FADH^{-}$ states, whereas the FAD^{ox} state does not form a hydrogen bond with Asn378. Rather, Asn378 increases interactions with Trp382 as the corresponding hydrogen bond distance becomes shorter in the FAD^{ox} state optimized geometry. However, the distances between Asn378 and Trp382 are significantly shorter in our models as compared to the crystal structure (Table 2), indicating that we are likely to overestimate the corresponding interactions. The stronger interactions might result from insufficient geometry constraints allowing Trp382 to approach Asn378 upon a movement of the helical turn containing Glu363 away from the active site in the course of geometry optimization. On the other hand, dynamics of the protein, which is ignored in our modeling, may control interactions in the active site, enhancing the Asn378−N_5 interactions and weakening the Asn378−Trp382 interactions. The artifact of the B3LYP/6-31G* computational method cannot be excluded either.

Nonetheless, the optimized structures indicate that the hydrogen bonding network surrounding the isoalloxazine ring is sufficiently flexible to accommodate FAD photoreduction without any major conformational change. Only slight tilting of the Asn378 side chain together with small displacements of isoalloxazine was observed in the optimized structures as shown in Figure 4. Yet, the characterized changes clearly revealed enhanced interactions of Asn378 with N_5−H of the neutral $FADH^{\bullet}$ state. The Asn378−N_5 distance decreased significantly in the radical $FADH^{\bullet}$ state compared to the fully reduced $FADH^{-}$ state. Indeed, the neutral semiquinoid radical of

DOI: 10.1021/jacs.5b10533
J. Am. Chem. Soc. 2016, 138, 4368−4376

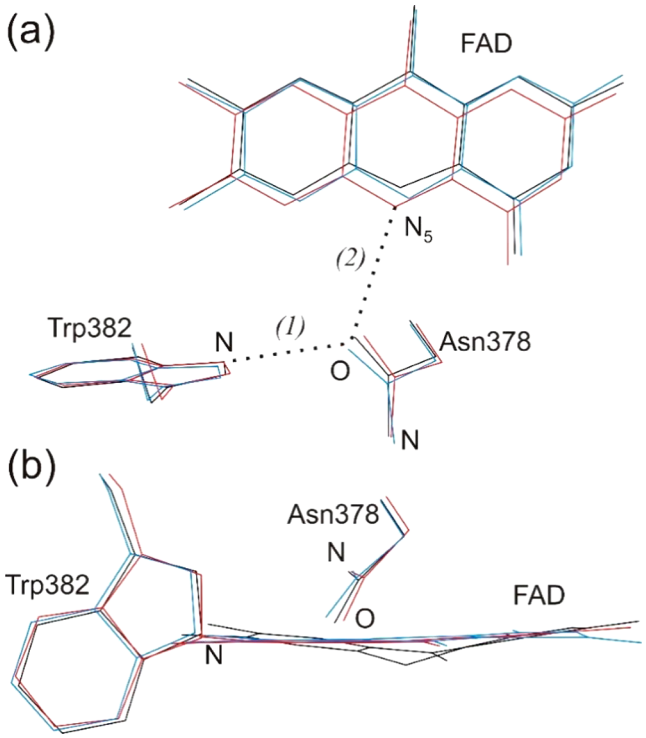

Figure 4. Interactions of Asn378 with flavin N_5 and Trp382 in three redox states. Structures were optimized with FAD^{ox} (blue), $FADH^{\bullet}$ (red), and $FADH^{-}$ (black). Two different views are presented in (a) and (b). Dotted lines indicate hydrogen bonds for which the distances are given in Table 2.

Table 2. Interatomic Distances (in Å) Characterizing Interactions in the Flavin Binding Pocket

distance	FAD^{ox}	$FADH^{\bullet}$	$FADH^{-}$	crystal structure PDB ID: 1DNP (molecule A/B)
Asn378–Trp382 (1)[a]	2.86	3.10	2.89	3.62/3.62
Asn378–N_5 (2)[a]	3.57	2.92	3.40	3.33/3.30
Arg344–N_5	3.93	4.22	3.31	3.42/3.47

[a]Distances (1) and (2) are indicated in Figure 4.

isoalloxazine is a better hydrogen-bond donor than negatively charged hydroquinone: the partial positive charge on the hydrogen of N_5–H is larger in the semiquinone $FADH^{\bullet}$ state (Mulliken charge 0.41 au) than in the hydroquinone $FADH^{-}$ state (Mulliken charge 0.36 au). Apparently, the role of the Asn378 side chain as part of the hydrogen-bonding network is to accept a stronger hydrogen bond from the $FADH^{\bullet}$ radical thereby stabilizing it. Remarkably, anionic $FADH^{-}$ interacts with the positively charged arginine Arg344 located at the bottom of the flavin binding pocket (not shown in Figure 4) by undergoing a butterfly bend toward Arg344 and away from Asn378.

To verify our models against the FTIR experimental data, we computed IR spectra using normal-mode analysis in the harmonic approximation. To be consistent with the experimental procedure, in addition to the natural isotope calculations, we performed uniform ^{13}C and Asn378 reverse ^{12}C labeling of our models. The computed difference IR spectra for FAD^{ox} and $FADH^{\bullet}$ reduction are shown in Figure 5. The assignments of all computed frequencies in the region of the

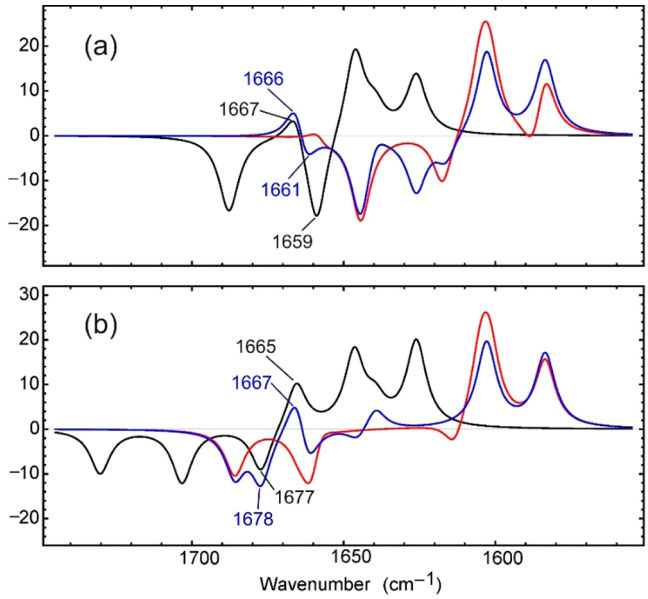

Figure 5. Computed difference IR spectra of flavin photoactivation. (a) $FADH^{-}$ minus $FADH^{\bullet}$; (b) $FADH^{-}$ minus FAD^{ox}. Unlabeled (black), uniform ^{13}C labeling (red), and reverse ^{12}C labeling of Asn378 (blue). Numbers indicate the frequencies (in cm^{-1}) of the bands assigned to the C=O group of Asn378. Assignments of other computed bands are indicated in the Supporting Information Table S1. IR intensity is in Debye/AMU·Å^2.

double bond stretches is presented in Supporting Table S1. Our computed difference IR spectra are in excellent agreement with our experimental FTIR spectra and fully support the experimental assignments. In particular, we found the Asn378 C=O stretch at 1659 cm^{-1} in the $FADH^{\bullet}$ state. Upon $FADH^{\bullet}$ reduction to $FADH^{-}$, the Asn378 C=O frequency upshifts to 1667 cm^{-1}. In the oxidized FAD^{ox} state, the Asn378 C=O stretch is found at 1677 cm^{-1}; it downshifts to 1665 cm^{-1} in the $FADH^{-}$ state. In Supporting Figures S6 and S7, we present our calculations for the FAD^{ox} model with the rotated Asn378 side chain. The calculations indicate that upon FAD^{ox} to $FADH^{-}$ reduction accompanied by Asn378 side chain rotation, a larger shift of the Asn signal than that identified in the FTIR spectra presented in Figure 2 should be expected. The results of the computational models without Asn378 rotation are in better agreement with the results of our FTIR experiments.

The agreement of the computed and experimental Asn378 C=O frequencies allows us to conclude that intermolecular interactions and geometries in our computational models correspond well with those involved in the experimentally observed $FADH^{\bullet}$ stabilization. Hence, we used the active site models to characterize the flavin redox potential. In particular, we compared the energies that characterize $FADH^{\bullet}$ to $FADH^{-}$ reduction crucial for the DNA repair function. As previously demonstrated by experimental studies, this reduction step requires the presence of the N_5-proximal Asn side chain,[24] and does not occur in the *E. coli* photolyase with mutated Asn378.[23] We compared the energies computed in the two redox states of interest $FADH^{\bullet}$ and $FADH^{-}$ at the two geometries optimized in these states (altogether four energies for each model) listed in Table 3. The flavin redox potential is defined through three relative energies as described in Computational Details, also listed in Table 3: the adiabatic electron affinity (AEA) of the $FADH^{\bullet}$ radical and reorganization energies λ_1 and λ_2 computed

DOI: 10.1021/jacs.5b10533
J. Am. Chem. Soc. 2016, 138, 4368–4376

Table 3. Computed Energies Characterizing FADH• to FADH⁻ Reduction

	models		
computed energies	Asn378	Ala378	LfH−6H_2O
(U)B3LYP/6-31G* energies,[a] Hartree			
FADH•//FADH•	−8991.382528	−8822.710777	−1330.573747
FADH⁻//FADH•	−8991.299625	−8822.641125	−1330.631898
FADH•//FADH⁻	−8991.358029	−8822.686424	−1330.550294
FADH⁻//FADH⁻	−8991.328457	−8822.667849	−1330.654541
Relative energies,[b] kcal/mol			
AEA	−33.9	−26.9	50.7
λ_1	18.1	16.8	14.2
λ_2	15.3	15.3	14.7

[a]Specified by the state of energy calculation//state of geometry optimization. [b]Defined in the Computational Details subsection.

in the FADH⁻ and FADH• states, respectively. To elucidate the role of Asn378−N_5 interactions, we carried out energy calculations of models with Asn378 substituted by Ala. In addition, we computed the radical and fully reduced states of hydrated lumiflavin LfH−6H_2O. A comparison of the photolyase models with the LfH−6H_2O model highlights the role of protein in setting the flavin redox potential.

We found a substantial difference in the semiquinone reduction energy when the photolyase models were compared to lumiflavin in water, indicating a pivotal role of apoprotein in determining the flavin redox potential. In the protein models, the energy of the FADH• state is significantly lower than the energy of fully reduced FADH⁻, which is reflected by the negative AEA in Table 3, − 33.9 and −26.9 kcal/mol in the Asn378 and Ala378 models, respectively. According to these AEA energies, the FADH⁻ state is thermodynamically unstable in photolyase. In vast contrast, reduction of hydrated lumiflavin LfH• to LfH⁻ is thermodynamically favored according to the positive AEA of 50.7 kcal/mol in Table 3. The positive AEA corresponds to the negative reaction energy (or negative free energy). Consistent with our estimate, the negative free energy of lumiflavin reduction from neutral semiquinone to anionic hydroquinone was determined in previous theoretical studies.[36,37] From this comparison of the protein models with lumiflavin in water, we conclude that the intrinsic electron affinity of isoalloxazine is drastically reduced in the photolyase active site by the flavin−protein interactions. The anionic groups such as deprotonated phosphates of FAD and carboxylates of Glu363, Asp372 and Asp374 close to isoalloxazine increase the energy of the anionic FADH⁻ state. Furthermore, the U-turn conformation of FAD accommodating phosphate groups close to isoalloxazine may play a role in redox tuning.

The high energy of the FADH⁻ state indicates that an energy barrier stabilizes this state kinetically in *E. coli* photolyase. To study this kinetic stabilization, we approximated the energies of the FADH• and FADH⁻ states with Marcus parabolas as described in Computational Details. Figure 6 shows the resulting energy diagram. To explain stabilization of the FADH• state, it is convenient to choose the energy of the FADH⁻ state at its optimized geometry as the zero energy. The black and blue parabolas represent the energies of the FADH⁻ and FADH• states, respectively, along the reduction/oxidation reaction coordinate. The red parabola represents the energy of excited FADH•*, which is upshifted with respect to the blue FADH• parabola by the excitation energy of 44 kcal/mol

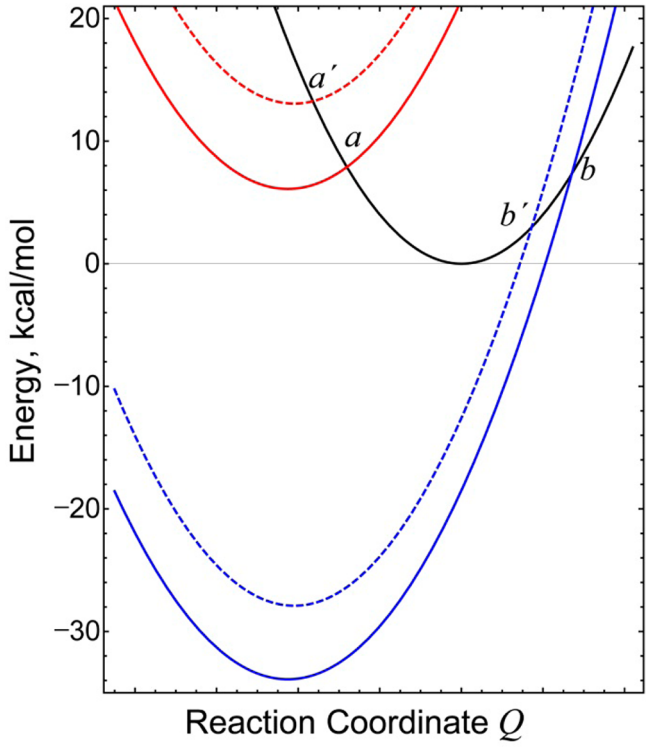

Figure 6. Kinetic stabilization of FADH⁻ by interactions with Asn378. The parabolas represent energies of semiquinone FADH• (blue), fully reduced FADH⁻ (black), and photoexcited semiquinone FADH•* (red) in the Asn378 model (solid line) and in the Ala378 model (dashed line). Thermodynamic stabilization of FADH• by Asn378 is linked with kinetic stabilization of FADH⁻.

corresponding to a 650 nm absorbance maximum. The three parabolas feature the complete electron transfer cycle consisting of forward electron transfer reducing FADH• or FADH•* to FADH⁻ and backward electron transfer oxidizing FADH⁻ to FADH•. The points at which the parabolas cross define the reduction/oxidation energy barriers. To elucidate the impact of interactions between Asn378 and N_5−H, we compared the energies of the Ans378 model (solid lines) with the energies of the Ala378 model (dashed lines).

In Figure 6, photoinduced reduction of FADH•* to FADH⁻ corresponds to Marcus normal region, whereas backward electron transfer that recovers FADH• from FADH⁻ falls into Marcus inverted region[38] defined by the condition −AEA > λ_2. In the inverted Marcus region, a larger negative AEA value increases the backward electron transfer energy barrier (the energy at which the black and blue parabolas intersect), leading to kinetic stabilization of the FADH⁻ state. Interactions with Asn378 instead of Ala378 increase the negative AEA value by 7.0 kcal/mol, which increases the backward electron transfer energy barrier by 4.5 kcal/mol. Thus, Figure 6 demonstrates that mutation of Asn378 to Ala should result in accelerated photoinduced electron transfer (barrier a′ in Figure 6) and rapid backward electron transfers without accumulation of FADH⁻ (barrier b′). The enhanced hydrogen bond of Asn378 with N_5−H in the FADH• state ensures thermodynamic stabilization of the FADH• state and kinetic stabilization of the FADH⁻ state (barrier b).

DOI: 10.1021/jacs.5b10533
J. Am. Chem. Soc. 2016, 138, 4368−4376

CONCLUSIONS

Combining our experimental and computational results, we conclude that photoactivation of photolyase is ensured via the acceptance of a single hydrogen bond, from the flavin N_5−H to the C═O group of Asn378, that relies on the better hydrogen bond donating property of the flavin semiquinone radical compared to the fully reduced flavin hydroquinone anion. In the FTIR spectra, the enhanced hydrogen bond from N_5−H to the protein is revealed by the 10 cm^{-1} downshifted Asn C═O stretching frequency in the $FADH^•$ state (1666 cm^{-1}), as compared to the frequency in the $FADH^-$ state (1677 or 1673 cm^{-1}). In the fully oxidized state FAD^{ox}, the Asn C═O stretch is instead upshifted (1688 cm^{-1}). The lack of change for C−N stretches eliminates the possibility of a rotational flip of the Asn378 side chain. The identified spectral shifts suggest that, upon light-induced FAD reduction, Asn378 tilts its amide side chain. The sub-Å differences induced by Asn378 tilting and $FADH^-$ bending were identified and characterized with the help of quantum-chemical calculations. These calculations also revealed significant thermodynamic destabilization of the $FADH^-$ state in the *E. coli* photolyase active site, due to interactions with several negatively charged groups close to the isoalloxazine ring. The $FADH^-$ destabilization facilitates backward electron transfer, preventing $FADH^-$ accumulation. Functionally important accumulation of the $FADH^-$ state is likely to be achieved by means of kinetic stabilization in the Marcus inverted region. The flavin N_5H − Asn378 hydrogen bond plays a central role in this stabilization. Enhanced hydrogen bonding with the $FADH^•$ radical increases thermodynamic stabilization of the radical state, and simultaneously ensures kinetic stabilization and accumulation of the fully reduced $FADH^-$ state.

On the basis of sequence conservation and structural similarities, the $FADH^•$ stabilization by an N_5 hydrogen bond with the proximal residue could likewise be proposed for (6−4) photolyases,[39,40] animal-like cryptochrome aCRY,[13] and DASH cryptochrome.[41,42] Moreover, stabilization of the flavin radical state by N_5−H hydrogen bonding to the protein could also contribute to redox tuning of flavoproteins that do not show light-dependent activation. In the crystal structures of the redox protein flavodoxin, the distance corresponding to a hydrogen bond between a backbone carbonyl and the N_5−H group was found to decrease in the neutral semiquinone state of the flavin mononucleotide cofactor $FMNH^•$ as compared to the fully reduced $FMNH^-$ state.[43] The functional relevance of this redox modulated interaction in flavodoxin was confirmed by mutagenesis studies.[44]

ASSOCIATED CONTENT

Supporting Information

The Supporting Information is available free of charge on the ACS Publications website at DOI: 10.1021/jacs.5b10533.

Light induced UV−vis spectra of CPD photolyase FAD activation from semiquinoid ($FADH^•$) and fully oxidized (FAD^{ox}) form into fully reduced ($FADH^-$) form; double difference FTIR spectra of semiquinoid ($FADH^•$) and fully reduced ($FADH^-$); description of the active site models and the LfH−$6H_2O$ complex, computational results of the FAD^{ox} model containing rotated Asn378 and the assignments of the computed frequencies in the double bond stretching region. (PDF)

AUTHOR INFORMATION

Corresponding Authors

*tatjana.domratcheva@mpimf-heidelberg.mpg.de
*kandori@nitech.ac.jp

Author Contributions

#IM.M.W. and T.D. contributed equally to this work.

Notes

The authors declare no competing financial interest.

ACKNOWLEDGMENTS

IM.M.W. thanks Dr. Junpei Yamamoto (Osaka Univ.) for fruitful discussions. T.D. is very grateful to Alex Granovsky (Firefly project) for advice and kind help with the numerical Hessian calculations. This work was supported by the MPG Minerva program (to T.D.) and "Research Unit Invitation" by Nagoya Institute of Technology (to T.D.).

REFERENCES

(1) Douki, T.; Reynaud-Angelin, A.; Cadet, E.; Sage, E. *Biochemistry* **2003**, *42*, 9221.
(2) Sinha, R. P.; Hader, D. P. *Photochem. Photobiol. Sci.* **2002**, *1*, 225.
(3) Kim, S. T.; Sancar, A. *Photochem. Photobiol.* **1993**, *57*, 895.
(4) Sancar, A. *Chem. Rev.* **2003**, *103*, 2203.
(5) Weber, S. *Biochim. Biophys. Acta, Bioenerg.* **2005**, *1707*, 1.
(6) Sancar, A.; Sancar, G. B. J. *J. Mol. Biol.* **1984**, *172*, 223.
(7) Todo, T.; Kim, S. T.; Hitomi, K.; Otoshi, E.; Inui, T.; Morioka, H.; Kobayashi, H.; Ohtsuka, E.; Toh, H.; Ikenaga, M. *Nucleic Acids Res.* **1997**, *25*, 764.
(8) Jorns, M. S.; Sancar, G. B.; Sancar, A. *Biochemistry* **1984**, *23*, 2673.
(9) Eker, A. P. M.; Hessel, J. K. C.; van de Velde, J. *Biochemistry* **1988**, *27*, 1758.
(10) Berg, B. J. V.; Sancar, G. B. J. *J. Biol. Chem.* **1998**, *32*, 20276.
(11) Byrdin, M.; Eker, A. P.; Vos, M. H.; Brettel, K. *Proc. Natl. Acad. Sci. U. S. A.* **2003**, *100*, 8676.
(12) Payne, G.; Heelis, P. F.; Rohrs, B. R.; Sancar, A. *Biochemistry* **1987**, *26*, 7121.
(13) Kato, R.; Hasegawa, K.; Hidaka, Y.; Kuramitsu, S.; Hoshino, T. *J. Bacteriol.* **1997**, *179*, 6499.
(14) Spexard, M.; Thöing, C.; Beel, B.; Mittaq, M.; Kottke, T. *Biochemistry* **2014**, *53*, 1041.
(15) Immeln, D.; Schlesinger, R.; Heberle, J.; Kottke, T. *J. Biol. Chem.* **2007**, *282*, 21720.
(16) Wijaya, I M. M.; Zhang, Y.; Iwata, T.; Yamamoto, J.; Hitomi, K.; Iwai, S.; Getzoff, E. D.; Kandori, H. *Biochemistry* **2013**, *52*, 1019.
(17) Hemmerich, P.; Nagelschneider, G. *FEBS Lett.* **1970**, *8*, 2.
(18) Xu, L.; Zhu, G. J. *J. Nucleic Acids* **2010**, *2010*, 794742.
(19) Todo, T.; Ryo, H.; Yamamoto, K.; Toh, H.; Inui, T.; Ayaki, H.; Nomura, T.; Ikenaga, M. *Science* **1996**, *272*, 109.
(20) Huang, Y.; Baxter, R.; Smith, B. S.; Partch, C. L.; Colbert, C. L.; Deisenhofer, J. *Proc. Natl. Acad. Sci. U. S. A.* **2006**, *103*, 11701.
(21) Kanai, S.; Kikuno, R.; Toh, H.; Ryo, H.; Todo, T. *J. Mol. Evol.* **1997**, *45*, 535.
(22) Kiontke, S.; Geisselbrechh, Y.; Pokorny, R.; Carell, T.; Batschauer, A.; Essen, L. O. *EMBO J.* **2011**, *30*, 4437.
(23) Hitomi, K.; Arvai, A. S.; Yamamoto, J.; Hitomi, C.; Teranishi, M.; Hirouchi, T.; Yamamoto, K.; Iwai, S.; Tainer, J. A.; Hidem, J.; Getzoff, E. D. *J. Biol. Chem.* **2012**, *30*, 4437.
(24) Damiani, M. J.; Nostedt, J. J.; O'Neill, M. A. *J. Biol. Chem.* **2011**, *286*, 4382.
(25) Xu, L.; Mu, W.; Ding, Y. *Biochemistry* **2008**, *47*, 8736.
(26) Burney, S.; Wenzel, R.; Kottke, T.; Roussel, T.; Hoang, N.; Bouly, J. P.; Bittl, R.; Heberle, J.; Ahmad, M. *Angew. Chem., Int. Ed.* **2012**, *51*, 9356.
(27) Siebert, F. *Methods Enzymol.* **1995**, *246*, 501.
(28) Masuda, S.; Hasegawa, K.; Ishii, A.; Ono, T. A. *Biochemistry* **2004**, *43*, 5304.

DOI: 10.1021/jacs.5b10533
J. Am. Chem. Soc. 2016, 138, 4368−4376

(29) Iwata, T.; Nozaki, D.; Tokutomi, S.; Kagawa, T.; Wada, M.; Kandori, H. *Biochemistry* **2003**, *42*, 8183.
(30) Barth, A. *Prog. Biophys. Mol. Biol.* **2000**, *74*, 141.
(31) Wijaya, I M. M.; Iwata, T.; Yamamoto, J.; Hitomi, K.; Iwai, S.; Getzoff, E. D.; Kennis, J. T. M.; Mathes, T.; Kandori, H. *Biochemistry* **2014**, *53*, 5864.
(32) Park, H. W.; Kim, S. T.; Sancar, A.; Deisenhofer, J. *Science* **1995**, *268*, 1866.
(33) Granovsky, A. Firefly Version 8, http://classic.chem.msu.su/gran/firefly/index.html, accessed September 2015.
(34) Schmidt, M. W.; Baldridge, K. K.; Boatz, J. A.; Elbert, S. T.; Gordon, M. S.; Jensen, J. H.; Koseki, S.; Matsunaga, N.; Nguyen, K. A.; Su, S.; Windus, T. L.; Dupuis, M.; Montgomery, J. A. *J. Comput. Chem.* **1993**, *14*, 1347−1363.
(35) Venyaminov, S. Yu.; Kalnin, N. N. *Biopolymers* **1990**, *30*, 1243.
(36) Kılıç, M.; Ensing, B. *J. Chem. Theory Comput.* **2013**, *9*, 3889.
(37) North, M. A.; Bhattacharyya, S.; Truhlar, D. G. *J. Phys. Chem. B* **2010**, *114*, 14907.
(38) Marcus, R. A.; Sutin, N. *Biochim. Biophys. Acta, Rev. Bioenerg.* **1985**, *265*, 811.
(39) Maul, M. J.; Barends, T. R.; Glas, A. F.; Cryle, M. J.; Domratcheva, T.; Schneider, S.; Schlichting, I.; Carell, T. *Angew. Chem., Int. Ed.* **2008**, *47*, 10076.
(40) Hitomi, K.; DiTacchio, L.; Arvai, A. S.; Yamamoto, J.; Kim, S. T.; Todo, T.; Tainer, J. A.; Iwai, S.; Panda, S.; Getzoff, E. D. *Proc. Natl. Acad. Sci. U. S. A.* **2009**, *106*, 6962.
(41) Brudler, R.; Hitomi, K.; Daiyasu, H.; Toh, H.; Kucho, K.; Ishiura, M.; Kanehisa, M.; Roberts, V. A.; Todo, T.; Tainer, J. A.; Getzoff, E. D. *Mol. Cell* **2003**, *11*, 59.
(42) Pokorny, R.; Klar, T.; Hennecke, U.; Carell, T.; Batschauer, A.; Essen, L. O. *Proc. Natl. Acad. Sci. U. S. A.* **2008**, *105*, 21023.
(43) Watt, A.; Tulinsky, A.; Swenson, R. P.; Watenpaugh, K. D. *J. Mol. Biol.* **1991**, *218*, 195.
(44) Ludwig, M. L.; Pattridge, K. A.; Metzger, A. L.; Dixon, M. M.; Eren, M.; Feng, Y.; Swenson, R. P. *Biochemistry* **1997**, *36*, 1259.

DOI: 10.1021/jacs.5b10533
J. Am. Chem. Soc. 2016, 138, 4368−4376